

Mechanical and corrosion properties of highly porous Ta-Nb-Sn alloy for intervertebral disc in spinal applications

Berk Atay, Ilven Mutlu*

Istanbul University-Cerrahpasa, Metallurgical and Materials Engineering Department, 34320, Istanbul, Turkey

In this study, low Young's modulus, highly porous Ta-Nb-Sn alloy foam was manufactured by using the space holder method. The aim of this study is development of an alloy with high wear resistance, with Young's modulus, with good imaging (MRI, CT) properties, and with high bioactivity. Ta alloy foam can be used in spinal applications (intervertebral disc) or dental applications. The space holder method enables the manufacturing of open-cell foam with a low elastic modulus. Powder mixtures were prepared through mechanical alloying. Carbamide was used to form pores. Ta has suitable strength, ductility, corrosion resistance, and biocompatibility. Ta has high price, however, and a high melting temperature, high activity, and high density. Nb addition lowered the melting temperature, elastic modulus, and cost of using Ta. The sinterability of Ta was enhanced by Sn addition. The corrosion behaviour of Ta alloy was examined. Young's modulus was determined by compression and ultrasonic tests. Tomography and radiography tests were also used.

Keywords: *metal foam, Ta-Nb-Sn, spinal implant, intervertebral disc, powder metallurgy*

1. Introduction

An open, porous structure is important in hard tissue implant applications because it mechanically anchors the implant to the bone. Highly porous structure can enhance the mechanical stability of the implant through bone growth inside the pores. The amount of porosity can reduce the elastic modulus of the implant [1–5]. Tantalum (Ta) is a refractory metal with a melting temperature of 2960°C. It has high strength, ductility, electrochemical corrosion resistance, and biocompatibility. In addition, Ta shows higher bioactivity than titanium (Ti) alloys. Ta₂O₅ film on the tantalum is inert to body fluids, which makes tantalum ideal for biomedical implant applications. Ta-based implants have been employed in medical applications without any problems. As Ta is a radiopaque metal and also a bioinert metal, it can be employed in marker balls in coronary stents. Marker balls are used in order to track the stents inside the body [6–10]. Ta has high price, however, as well as high density, and manufacturing Ta-based parts is difficult because of its high melting temperature and affinity for

oxygen. Nb and Sn additions to Ta can reduce the melting temperature, the elastic modulus, and the cost. In addition, artefacts and medical image distortions are low in Ta-based implants [9–12].

The human spinal (vertebral) column, known as the backbone, contains 33 vertebrae that are joined by intervertebral discs, ligaments, and facet joint capsules (connective tissue). The vertebral column is important in movement, protects the spinal cord, carries the body weight, and forms the axis of the body. The vertebral column is curved in several places, a result of human bipedal evolution. The curves allow the human spine to better stabilize the body. The intervertebral disc (intervertebra fibrocartilage) is a complicated bone-like/cartilage tissue. The main function of the intervertebral disc (IVD) is to show resistance to external forces in the spine. The IVD provides impact absorption properties to the spine and the body. The spinal column is anatomically defined by the vertebrae, intervertebral discs, ligaments/muscles, and nervous system. Interbody fusion is a surgical operation for spinal diseases. Interbody fusion includes positioning of a cage/graft in the intervertebral space after discectomy. Intervertebral disc is a cartilage-like material between the adjacent

* E-mail: imutlu@iuc.edu.tr

vertebrae in the spinal column. IVD consists of an outer fibrous ring, the annulus fibrosus (AF), which surrounds an inner gel-like centre, the nucleus pulposus (NP). AF and NP made up of collagen, water, and proteoglycans. AF consists of several layers of fibrocartilage. NP is a gelatinous tissue. Relatively stronger, AF acts like a coiled spring, while NP acts like a ball bearing (resists compression loads). An intervertebral disc functions to separate the vertebrae from each other and provides the surface for the shock-absorbing gel of the NP. In general, NP distributes the pressure in all directions within an intervertebral disc under compression. The disc shows viscoelastic character. Anterior cervical discectomy and fusion (ACDF) is an operation for disc diseases. Fusion can be carried out by using an autograft from the iliac crest. In addition, allografts (osteoconductive materials) can be used. In the normal position, body weight produces bending moments on the vertebra. As the vertebral column is an S-like curve, weight produces both compression force and shear force. Rotation of the vertebra also produces shear forces. Healthy disc distributes the loads homogeneously. In case of disc degeneration, disc distributes the loads unequally and loses its cushion ability. Highly porous Ta foam can be an alternative material for intervertebral discs. Ta foam is more osteoconductive than other metals, producing few artefacts in imaging. Titanium alloy-based cages are harder than bone and the cages can sink into the vertebral endplates. Ti causes MRI and CT artefacts that make it difficult to visualize the fusion constrict. In addition, Ta shows higher bioactivity than Ti and Ti alloys. Polyetheretherketone (PEEK) does not display the subsidence problem, and imaging of PEEK is good. PEEK is bioinert, however, and therefore does not show bioactivity [13].

Papacci et al. [13] studied anterior cervical discectomy and interbody fusion. Kasliwal et al. [14] studied failure of porous tantalum cervical interbody fusion devices. Mobb et al. [15] studied the literature and evidence for different lumbar-interbody fusion techniques. The authors of this report investigated the interbody fusion options. Xu et al. [16] studied MoSi₂ composite coating with a TaB₂ diffusion barrier on tantalum substrate. The

coating showed excellent oxidation resistance due to the prevention of diffusion of Si atoms. Hao et al. [17] prepared coatings on Ta-12W alloy in alkali electrolytes. The effect of electrolyte on the composition, morphology, and microstructure of the coating was investigated. The growth of the coating in phosphate is dominated by the oxidation of the substrate. The coatings prepared in the dual electrolyte exhibit superior wear resistance. Ma et al. [18] studied the influence of severe rolling on the dissolution rate of the Ta-4W sheet in different directions during immersion testing. The dissolution rate of the cold-rolled sample was significantly lower than in the undeformed sample. Severe rolling promotes grain subdivision accompanied by long boundaries. Browning et al. [19] studied the mechanical properties of pure Ta, Ta-10W, and Ta-10W-1.5TiC. Pure tantalum was found to display higher ductility. The addition of W and TiC was found to result in comparable high temperature strength and ductility, as well as improved hardness. Ma et al. [20] studied tantalum-tungsten alloys for high-temperature applications. To evaluate the mechanical properties of tantalum-tungsten alloys at elevated temperatures, binary Ta-W was chosen, and their mechanical properties were tested. Tensile stress, yield stress, and elongation gradually decrease, while the total tensile elongation remains constant as the temperature increases. Wang et al. [21] studied tantalum coating on titanium. An in vivo study was performed on diabetic sheep. Aguilar et al. [22] investigated the Ti-Ta-Sn alloys for biomedical applications, with a particular focus on their use in trabecular bone replacement. This work aims to analyse the influence that of Sn has on the mechanical properties and antibacterial response of ternary alloy foams. The alloys were obtained by means of mechanical alloying. The foams were obtained using NaCl as space holder and consolidated by a hot pressing. The foams exhibited homogeneous pore distribution with a pore size between 100 and 450 μm and with a porosity slightly higher than 50%. None of the foams showed antibacterial activity nor bacterial adhesion. Kuo et al. [23] studied vacuum plasma spraying in order to deposit Ta powder in three layers on Ti6Al4V substrates. In

the deposition, the melting rate of the Ta powder was controlled by regulating the spray power in such a way as to form a coating with a porosity that increased from the inner to the outer layer. Results obtained from biocompatibility tests showed that cells had better attachment and spreading on the Ta coating than on the Ti6Al4V sample.

In the present study, Ta-Nb-Sn alloy foam was manufactured for spinal implant (intervertebral disc) applications. The aim of the study was development of an alloy with high wear resistance, Young's modulus close to that of bone, with good medical imaging (MRI, CT) properties, and with high bioactivity and osseointegration properties. Highly porous open-cell foam-like structure was obtained by using the pore former–water leaching method. Nb addition to the Ta can reduce the melting temperature, elastic modulus, and the price of Ta alone. Sn is a nontoxic, solid solution strengthening element for the Ta. In addition, the melting temperature of Ta can be lowered by the Sn addition. Although there are studies on the porous materials for implant applications, there have been no reports on the use of porous Ta [6]. Although Ta-Nb alloys have been studied, there is no published work on the triple Ta-Nb-Sn alloy. Young's modulus of Ta-Nb-Sn alloy samples was determined by both compression and ultrasonic tests (destructive and nondestructive tests). Tomography and radiography tests were also employed. Wettability of the alloy was also characterized.

2. Experimental

2.1. Specimen production

Ta, Nb, and Sn powders, having a particle size of 30–40 μm , were employed as a raw material for the manufacturing of highly porous, foam-like Ta-Nb-Sn alloy samples. 5–35 %wt. Nb, 1–5% wt. Sn powders, and balanced Ta powders were mixed (Alfa Aesar, USA). Ta, Nb, and Sn powders and 3-mm ZrO_2 balls (metal/ball ratio of 10/1) were ball-milled for 6 hours. Rotation speed was 600 rpm. Carbamide (urea) was used as a pore-forming material. Some PVA (polyvinylalcohol) was added to the powder mixture for green strength

and compressibility. Mixtures were pressed at 200 MPa into cylindrical samples (12×20 mm). Samples were immersed into the water and then the carbamide (pore former) was removed. Ta-Nb-Sn alloys were sintered at 1400°C for 240 min in argon.

2.2. Mechanical properties and microstructure

Microstructure of the Ta-Nb-Sn alloy samples were investigated using field emission gun-scanning electron microscopy (FEG-SEM) (FEI Quanta). Mechanical properties were studied using compression tests (Devotrans, Turkey). Young's modulus was studied using the ultrasonic method (General Electric, USM-Go). As the wettability is important for orthopaedic implants, the contact angle of the Ta-Nb-Sn alloys was measured using optical tensiometer-contact angle meter (Attension Theta) by the sessile drop method.

Computed cone-beam-based tomography (Dental CT) was employed for imaging the pore structure. Samples were exposed to x-ray at 9 mA, 90 kV. Digital images were evaluated by a software (OnDemand3dDental). Tomography device was captured data by using x-ray beam (cone-beam based) during a 360° rotation around the Ta alloy.

In addition, digital radiography (DR) was employed for the investigation of the imaging properties. Samples were exposed to x-rays at 90 kV, 14.3 mA, for 10 seconds (Balteau). Phosphor imaging plates were employed (Flex, Carestream). Scanner was VMI 5100MS. Images were processed using Starrview software.

2.3. Static immersion tests

Simulated body fluid (SBF) solution was prepared with a composition of 8.00 (g/L) NaCl, 0.30 (g/L) CaCl_2 , 0.20 (g/L) KCl, 0.30 (g/L) MgCl_2 , 0.20 (g/L) K_2HPO_4 , 0.35 (g/L) NaHCO_3 , 0.07 (g/L) Na_2SO_4 , and some tris [24–30]. The pH was set to 7.40. Alloys were immersed into the SBF for up to 14 days. ICP-MS (Thermo Scientific) was employed to measure the metal ion release levels. Weight change values were determined using dry weight measurements.

2.4. Electrochemical corrosion tests

Electrochemical corrosion studies were carried out in the SBF solution using a potentiostat (Interface 1000, Gamry). Saturated calomel electrode (SCE) was the reference electrode, graphite was the counter electrode, and the Ta-Nb-Sn alloy was the working electrode. Open circuit potential (OCP) was measured for 7200 seconds. Linear polarization resistance (LPR) was employed to determine the polarization resistance and corrosion rate. Tafel curves were obtained by polarizing the Ta-Nb-Sn alloys with respect to the OCP.

2.5. Cytotoxicity evaluation

In the present study, *in vitro* evaluation of the cytotoxicity of the Ta-Nb-Sn alloys were studied by extraction-based 3T3 neutral red uptake (NRU) assay. The 3T3 NRU assay is based on the ability of living cells to uptake supravital neutral red dye, which can penetrate the cell membrane by nonionic diffusion. Neutral red (NR) is a weak cationic dye, with which living cells can be distinguished from dead cells. The NRU assay provides a quantitative estimation of the number of viable cells in a culture. Positive (sodium laureth sulfate) and negative (polypropylene) samples were prepared to verify the test system. Ta-Nb-Sn alloy test substances were exposed to an immortalised mouse fibroblast Balb/c 3T3 cell line. Absorbance (optical density) measurements were performed at 540 nm in order to determine the viability/survival. Cytotoxicity can be expressed as a reduction of the uptake of neutral red. Dulbecco's modification of Eagle's medium (DMEM) cell culture medium, bovine calf serum (BCS), trypsin/EDTA were the chemicals used. Serum culture medium (SCM) was used as the extraction agent because it supports extraction of polar and nonpolar substances and cell proliferation. The cell culture was removed from culture flasks using enzymatic digestion (trypsin/EDTA), and then the cell suspension was centrifuged. The cells were then resuspended and seeded at 10^4 cells per well in DMEM in a 96-well plate. After incubation, the culture was aspirated. After incubation, culture medium was removed, and the cells were washed with phosphate-buffered saline (PBS), The

test system is considered suitable if the viability for the negative specimen is $>70\%$ of the blank.

3. Results and discussion

3.1. Mechanical properties and microstructure

Highly porous open-cell Ta-Nb-Sn alloy foam-like samples were manufactured by the press-sinter-based pore former–water leaching route. Pore morphology of the sintered structures replicated the starting morphology and diameter of the urea (carbamide) particles. Figure 1 illustrates the SEM images of (a) Ta powder, (b) Nb powder, (c) Sn powder, and (d) carbamide. Figure 2 illustrates (a) photograph of the sintered Ta-Nb-Sn alloy foam, (b) SEM image of the macro-pores at the cracked surface of the sintered foam, (c) SEM image of the cell wall of the sample (low magnification), and (d) SEM image of the cell-wall of the sample (high magnification). Micropores in the microstructure due to incomplete sintering are not undesirable. Some micropores are important in the transportation of body fluids.

Table 1 shows the average sizes of the pore-former carbamide (urea) particles and the average pore diameter of the alloys. Mean pore size of the sintered specimen was $590 \mu\text{m}$, while mean particle size of the corresponding irregular

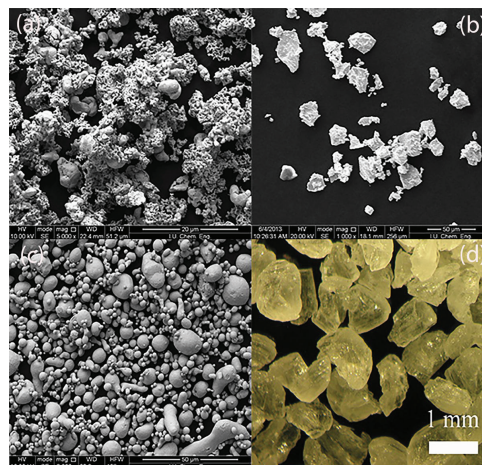


Fig. 1. SEM images of (a) Ta powder, (b) Nb powder, (c) Sn powder, and (d) carbamide powder

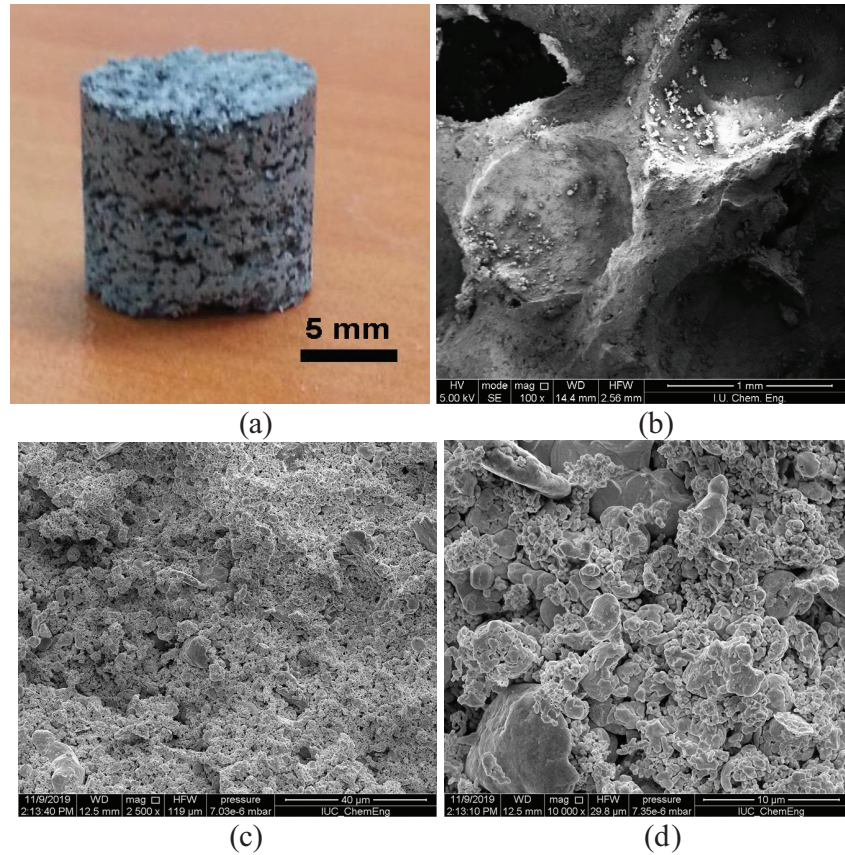


Fig. 2. (a) Photograph of the foam, (b) SEM image of the macro-pores, (c) SEM image of the cell wall (low magnification), and (d) SEM image of the cell wall (high magnification)

Table 1. Mean size of carbamide particles and mean pores size of the sintered foams

Carbamide particle shape	Carbamide particle size ranges (μm)	Mean carbamide particle size (μm)	Mean pore size (μm)
Irregular	-1400+1000	1270	850
Irregular	-1000+710	860	590
Irregular	-710+500	580	410
Spherical	-1400+1000	1300	880

carbamide pore former was $860 \mu\text{m}$. When pore-former carbamide with a mean particle size of $580 \mu\text{m}$ was used, a mean pore size of $410 \mu\text{m}$ was obtained in the sintered specimens. The final pore size value is associated to the pore-former carbamide size. Pore shape was also similar to the original pore-former carbamide (urea) morphology. The average diameter of the pore former

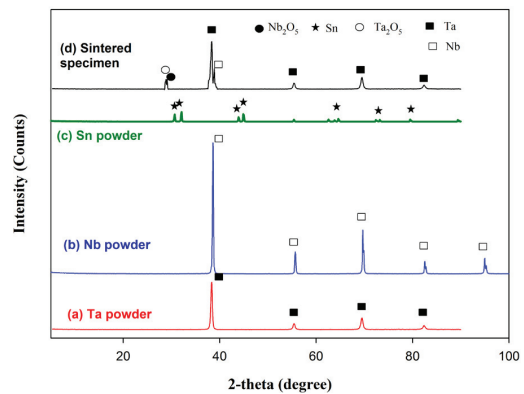


Fig. 3. XRD patterns of the (a) Ta powder, (b) Nb powder, (c) Sn powder and (d) sintered alloy

carbamide was slightly higher than the pores. The difference was attributed to crushing of the carbamide during pressing [1–5].

Figure 3 illustrates the x-ray diffraction (XRD) results of the powders (a) Ta, (b) Nb, (c) Sn powder

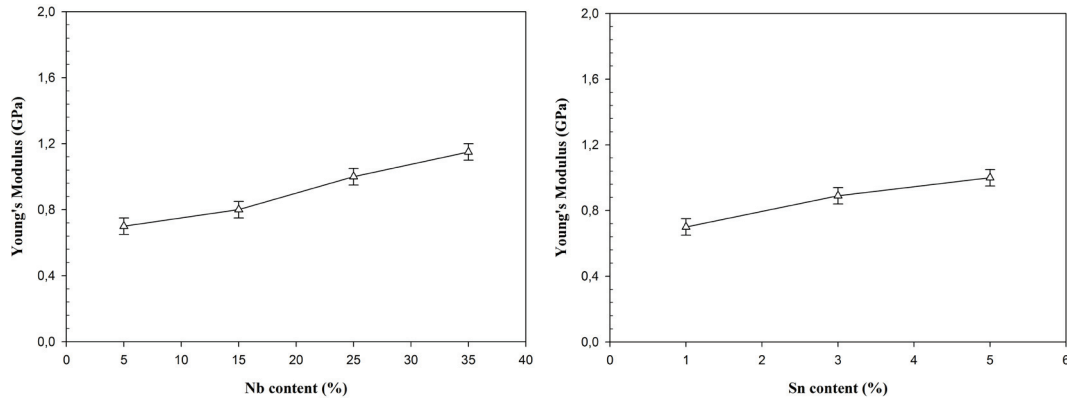


Fig. 4. Effect of (a) Nb content and (b) Sn content of the alloy on the Young's modulus

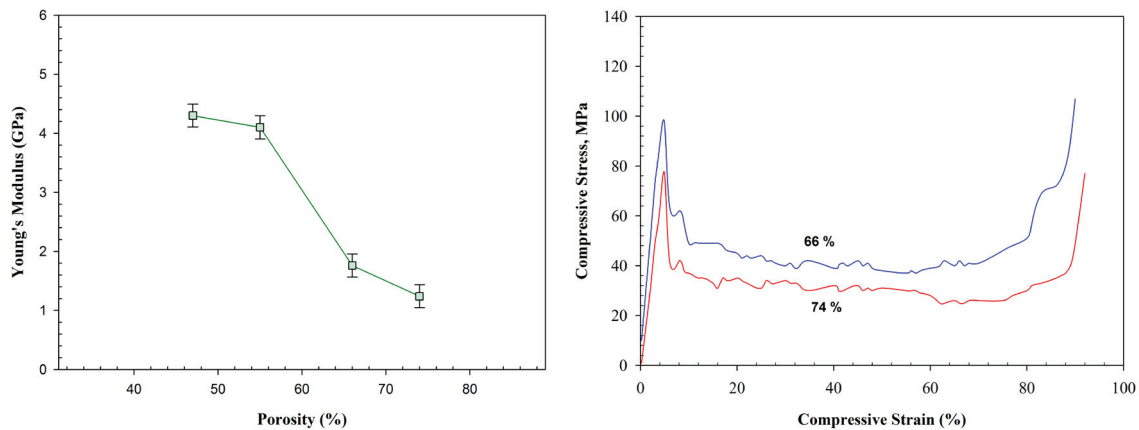


Fig. 5. Effect of porosity on (a) Young's modulus and (b) compressive stress–strain diagram

and (d) the sintered Ta-Nb-Sn alloy. As seen from the Figure 3(a), as-received Ta powder consists of Ta phase. As seen from Figure 3(d), the sintered sample consisted of Ta phase. Some oxides (Ta_2O_5 and Nb_2O_5) were also observed on the surfaces. Figure 4 illustrates the effect of (a) Nb content and (b) Sn content of the alloy on the elastic modulus of the about 70% porous samples.

Figure 5 illustrates the effect of the porosity level of the alloy on the (a) elastic modulus and (b) compressive stress-compressive strain curve. There are three regions in the curves: an elastic region, a plateau region, and a densification region. The plateau region is important for the energy/impact absorption properties. Yield strength values of the Ta-Nb-Sn alloys increased and the long plateau region get shortened with increasing Nb content.

Porosity content of the sintered specimens increasing from 46% to 74% caused the Young's modulus to decrease from 4.3 GPa to 1.3 GPa.

3.2. Corrosion tests

Figure 6 illustrates the change of OCP level with (a) Nb addition and (b) Sn addition. Raising the Nb content of the sample raised the OCP level, whereas raising Sn content slightly lowered the OCP. Tafel curves were employed to evaluate the corrosion performance. Figure 7 illustrates the effect of (a) Nb content of the Ta-Nb-Sn alloy and (b) Sn content of the Ta-Nb-Sn alloy on the Tafel curves. Increasing the Nb content of the samples increased their corrosion potential and decreased their corrosion current density.

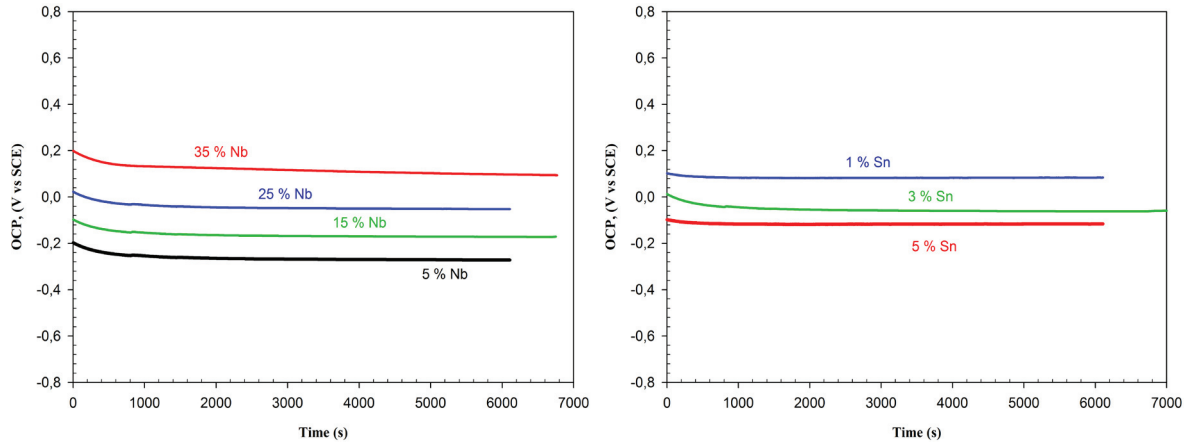


Fig. 6. Variation of the open circuit potential value with (a) the Nb content and (b) the Sn content of the alloy

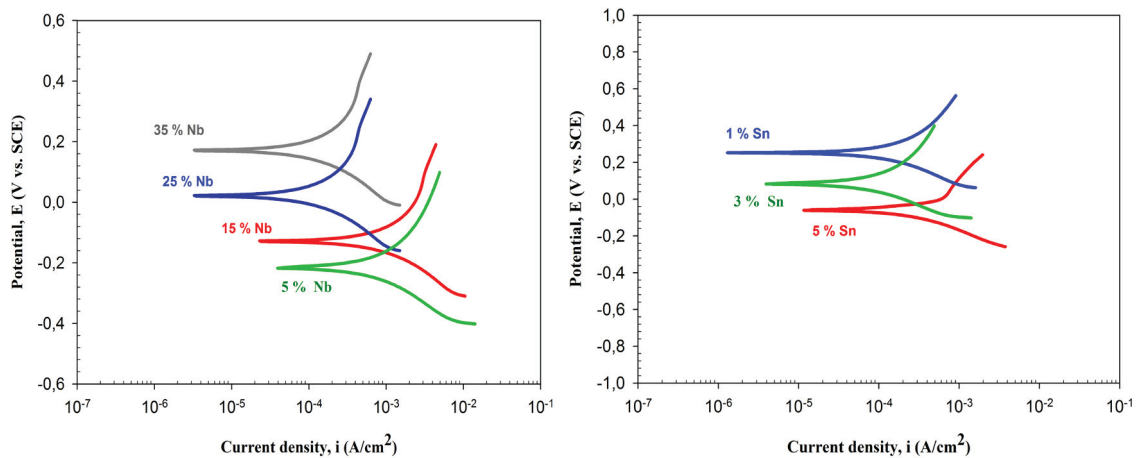


Fig. 7. Effect of (a) Nb content and (b) Sn content of the alloy on the Tafel curves of the samples

Increasing Sn content of the specimens decreased the corrosion resistance.

Figure 8 illustrates the effect of (a) Nb content of the alloy, (b) Sn content of the alloy, and (c) porosity of the specimen on the polarization resistance and corrosion rates. Polarization resistance of the samples increased with incorporation of Nb, and corrosion rate of the decreased with Nb addition. Sn addition lowered the polarization resistance of samples. Increasing Nb content of the alloy samples from 5% to 35%, decreased the electrochemical corrosion rate of the specimen from 3.2 mm/year to 2.0 mm/year. While increasing Sn content of the alloy from 1% to 5%, the electrochemical corrosion rate of the specimen increased

from 2.5 mm/year to 3.0 mm/year. In general, Ta is very inert and resists corrosion in acidic solutions. Only highly acidic solutions containing fluoride ions can corrode the Ta. The inert nature of Ta is ideal for biomedical implant purposes. The inert nature and biocompatibility of Ta is a consequence of the surface oxides. Ta has two types of oxide, Ta_2O_5 (more stable) and TaO_2 .

3.3. Static immersion test

Figure 9 illustrates the effect of the immersion time on (a) the weight change and (b) metal (Ta) ion release by Ta-35Nb-5Sn alloy in the simulated body fluid. As seen from Figure 9, weight change (loss) and metal (Ta) ion release values of

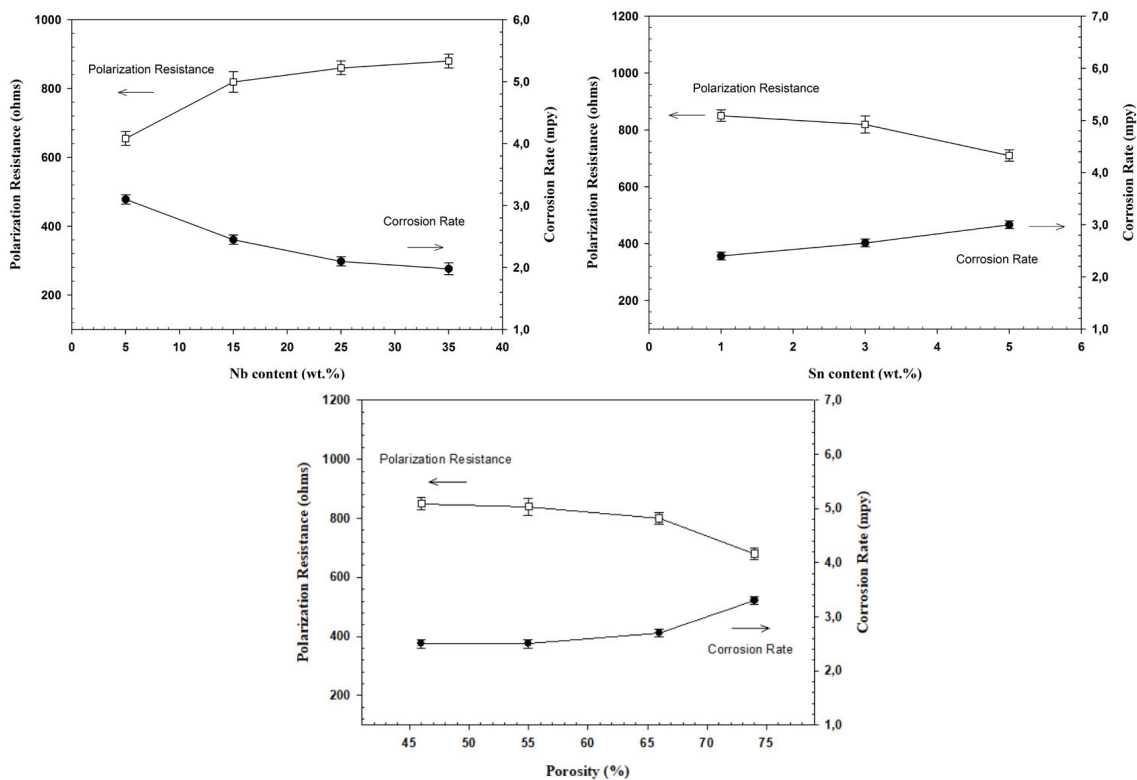


Fig. 8. Effect of (a) Nb content of the alloy, (b) Sn content of the alloy, and (c) porosity content on the polarization resistance and corrosion rate

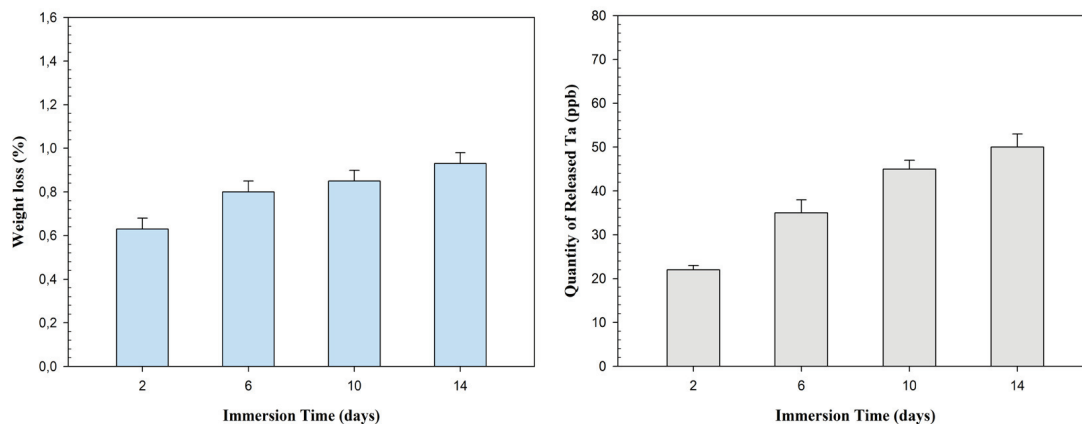


Fig. 9. Effect of immersion time on the (a) weight loss and (b) Ta ion release in simulated body fluid solution

the samples increased with time. Figure 10 illustrates the effect of the Nb addition on (a) weight change (loss) and (b) Ta ion release. As seen from Figure 10, weight loss and Ta ion release values

of the samples decreased with incorporation of Nb. Figure 11 illustrates the effect of Sn content of the alloy on the (a) weight change (loss) and (b) Ta ion release in the simulated body fluid. Weight loss and

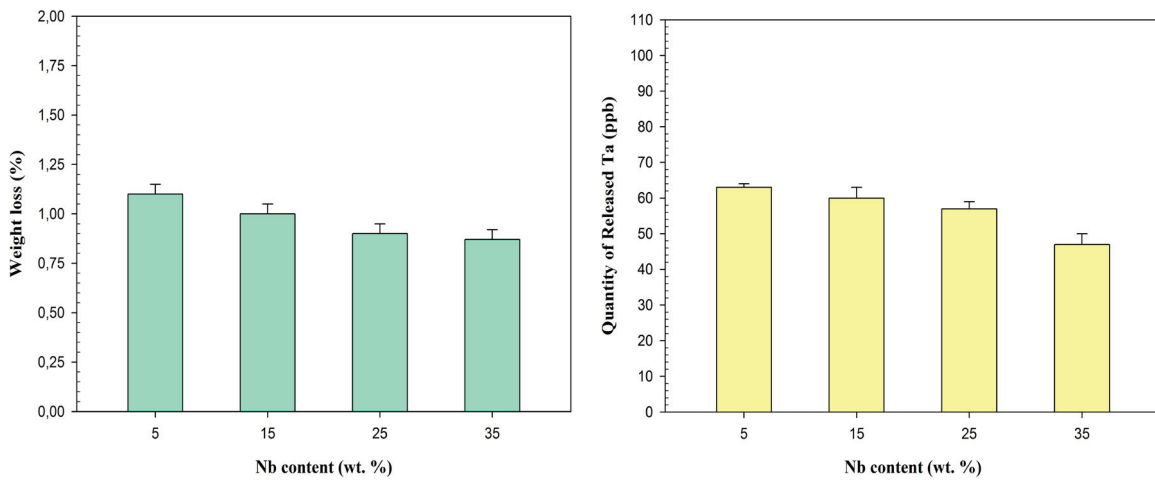


Fig. 10. Effect of Nb content of the alloy on (a) weight loss and (b) Ta ion release in simulated body fluid solution

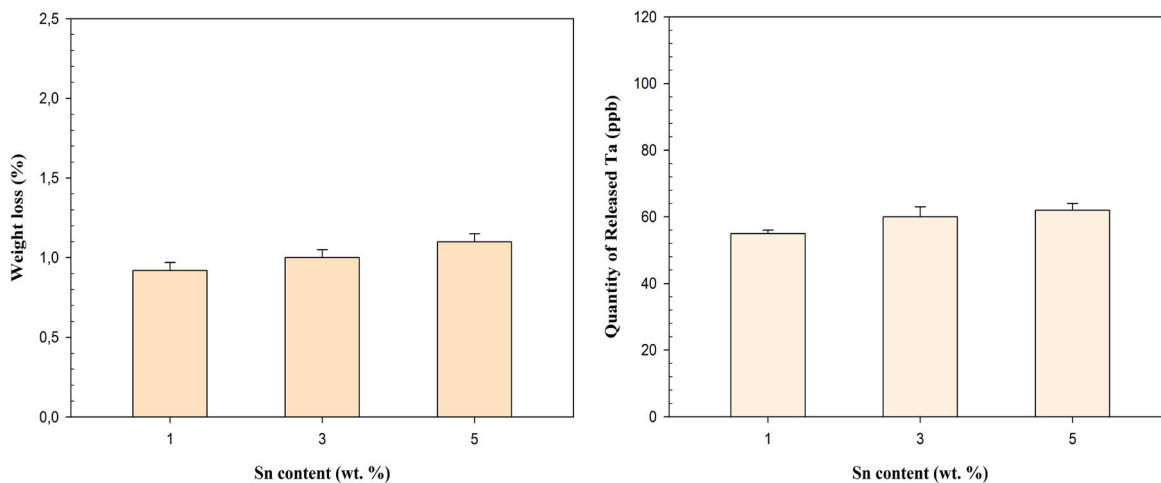


Fig. 11. Effect of Sn content of the alloy on the (a) weight loss and (b) Ta ion release in simulated body fluid solution

Ta release levels increased with the Sn addition. Figure 12 shows the effect of the porosity content of the Ta-35Nb-5Sn alloy on the (a) weight loss and (b) Ta ion release in simulated body fluid solution for 14 days. Increasing porosity content increased the weight loss and Ta ion release values of the specimens.

Wettability (contact angle) of the Ta-Nb-Sn alloys was studied by using optical tensiometer. The mean droplet (water) contact angle for the Ta-Nb-Sn alloys was about 80°. Figure 13 displays

a photograph of the droplet at the surface. As the contact angle is below 90°, the wettability of the Ta-Nb-Sn alloy is suitable.

3.4. Radiographic characterization

Computed tomography (CT) and digital radiography (DR) methods were employed for structure imaging. The tomography method was used for determination of pore structure and pore distribution, while the radiography method was used in

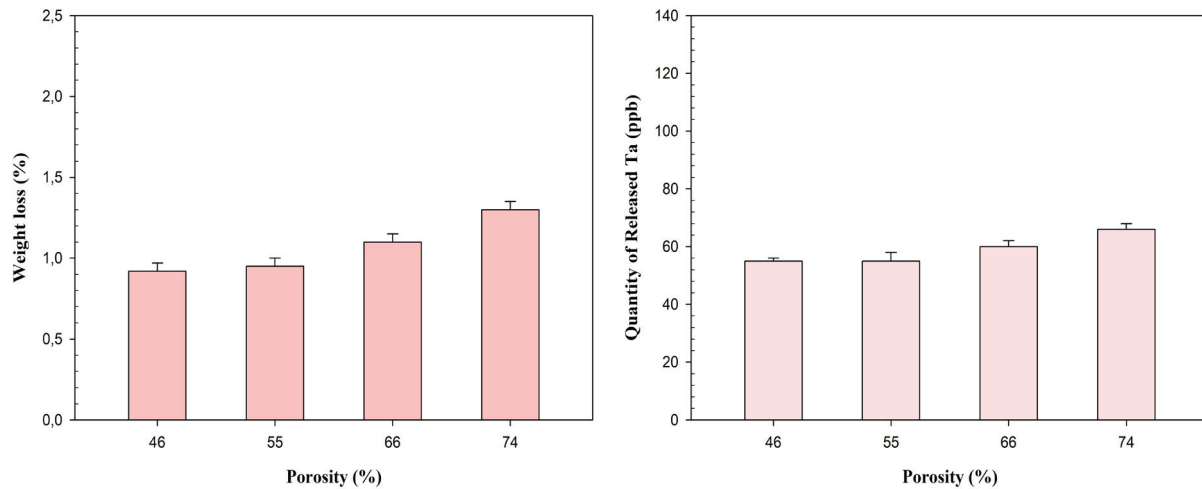


Fig. 12. Effect of porosity content of the alloy on (a) weight loss and (b) Ta ion release

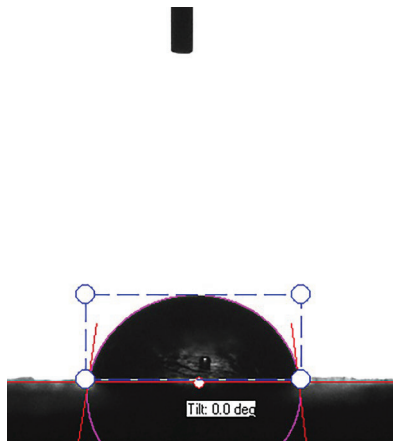


Fig. 13. Photograph of the water droplet at the surface of the sample

order to determine the radiopacity of the alloy. Figure 14 shows the images of the foams with 70% porosity in both (a) radiographic view and (b) tomography images. The Ta-Nb-Sn samples show suitable radiopaque behaviour. Radiopaque materials have a bright, white appearance on the radiographs, compared with the relatively darker appearance of the radiolucent materials. For example, bones or metals look white or light grey (visible or radiopaque), whereas polymers, tissue, and skin look black or dark gray (invisible or radiolucent). Implant materials must have radiopacity for

surgical operations. Macro or micro-cracks were not detected according to radiography. Figure 14(b) shows the 3D image of the 70% porous foam. The Ta-Nb-Sn foam consisted of homogeneously distributed open pores according to the tomography results.

In this study, evaluation of the cytotoxicity of the Ta-Nb-Sn alloy was performed with the 3T3 NRU assay. The assay is based on the ability of living cells to uptake neutral red dye, which can penetrate the cell membrane. Positive (sodium laureth sulphate) and negative (polypropylene) samples were prepared to verify the test system. Ta-Nb-Sn alloy test substances were exposed to immortalised mouse fibroblast Balb/c 3T3 cells. Ta alloy does not have cytotoxic potential. The viability value of Ta alloy was about 88%, which is not lower than the limit value (70%). This means that the Ta alloy has no cytotoxic potential.

4. Conclusions

This study presented a method for production of highly porous Ta alloy foam for spinal implant applications. In this work, the manufacturing of highly porous Ta-Nb-Sn alloy foam was carried out by using the press-sinter-based, space-holder method. Low elastic modulus open-cell Ta-Nb-Sn alloy foam can be used as material for

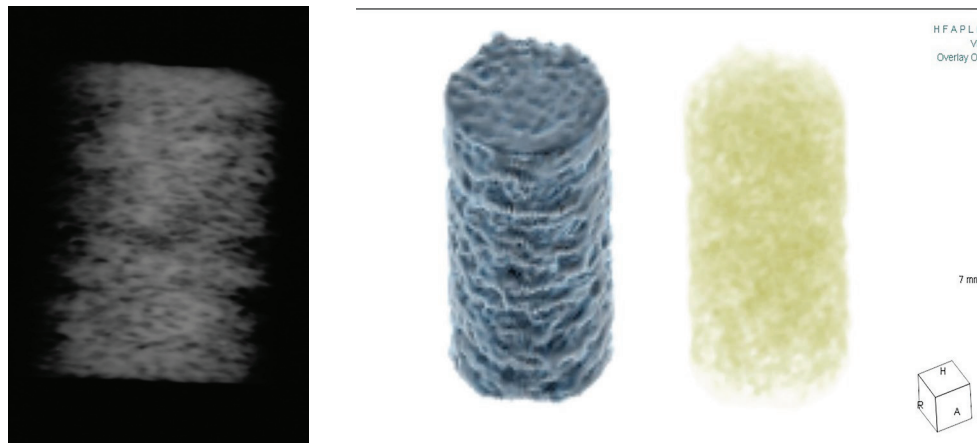


Fig. 14. (a) Digital radiography result of the sample and (b) computed tomography images of the sample

spinal implant. The space-holder sintering technique makes it possible to obtain an open-cell Ta foam-like structure with low elastic modulus close to cancellous bone. In addition, Ta shows higher bioactivity than Ti and Ti alloys. The powder mixtures were mechanically alloyed. Carbamide was employed as a pore-forming material. The pore sizes of the foams were similar to the initial size of the pore former. The mean pore size of the sintered specimen was $590\ \mu\text{m}$, whereas the mean particle size of the corresponding irregular carbamide pore former was $860\ \mu\text{m}$. When pore former carbamide with a mean particle size of $580\ \mu\text{m}$ was used, a mean pore size of $410\ \mu\text{m}$ was obtained in the sintered specimens. Increasing the porosity content of the sintered specimens from 48% to 74% decreased the Young's modulus from 4.3 GPa to 1.3 GPa. Corrosion behaviour of the alloys was evaluated in simulated body fluid. Corrosion resistance was enhanced with incorporation of the Nb. The corrosion rate of the samples was lowered with Nb addition. Increasing Nb content of the alloy from 5% to 35% decreased the electrochemical corrosion rate of the specimen from 3.2 mm/year to 2.0 mm/year, while increasing Sn content of the alloy from 1% to 5%, increased the electrochemical corrosion rate of the specimen from 2.5 mm/year to 3.0 mm/year. Weight loss and Ta ion release values of the samples were raised with immersion time. Meanwhile, weight change and Ta ion release values were lowered by raising

Nb. The contact angle of the Ta-Nb-Sn alloys was about 80° , which is suitable for spinal implant (intervertebral disc) applications. Radiography and tomography methods were used for 3-dimensional defect and structure characterization. The tomography method was used for determination of pore structure and pore distribution, while the radiography method was used in order to determine the radiopacity of the alloy. Ta-Nb-Sn samples show suitable radiopaque behaviour. Radiopaque materials have a bright, white appearance, compared with the darker appearance of the radiolucent materials. Bones or metals look white or light grey (visible or radiopaque), whereas polymers, and skin look dark grey (radiolucent). Implant materials must have radiopacity. The Ta-Nb-Sn foam consisted of homogeneously distributed open pores according to the tomography results. As a result, low elastic modulus open-cell Ta-Nb-Sn alloy foam-like structure can be used in the spinal implant applications.

Acknowledgment

This work was supported by Scientific Research Projects Coordination Unit of Istanbul University-Cerrahpasa, Project numbers 34943, 35631, and 35175.

References

- [1] Wenjuan W, Chenguang B, GuiBao Q, Qiang W. Processing and properties of porous titanium using space holder technique. *Mater Sci Eng A*. 2009;506:148–51.
- [2] Mutlu I, Oktay E. Characterization of 17-4 PH stainless steel foam for biomedical applications in simulated body

- fluid and artificial saliva environments. *Mater Sci Eng C*. 2013;33(3):1125–31.
- [3] Gibson LJ. Biomechanics of cellular solids. *J Biomech*. 2005;38:377–99.
- [4] Ashby MF, Evans AG, Fleck NA, LjGibson, Hutchinson JW, Wadley HNG. Metal foams: a design guide. Boston, MA: Elsevier Science; 2000.
- [5] Wang H, Li J, Yang H, Liu C, Ruan J. Fabrication, characterization and in vitro biocompatibility evaluation of porous Ta-Nb alloy for bone tissue engineering. *Mater Sci Eng C*. 2014;40:71–5.
- [6] Ruperez E, Manero JM, Riccardi K, Li Y, Aparicio C, Gil FJ. Development of tantalum scaffold for orthopedic applications produced by space-holder method. *Mater Des*. 2015;83:112–9.
- [7] Efe M, Kim HJ, Chandrasekar S, Trumble KP. The chemical state and control of oxygen in powder metallurgy Tantalum. *Mater Sci Eng A*. 2012;544:1–9.
- [8] Kim Y, Lee D, Hwang J, Ryu HJ, Hong SH. Fabrication and characterization of powder metallurgy tantalum components prepared by high compaction pressure technique. *Mater Charact*. 2016;114:225–33.
- [9] Adamek G, Jakubowicz J. Tantalum foam made with sucrose as a space holder. *IJRMHN=M*. 2015;53:51–5.
- [10] Yang H, Li J, Zhou Z, Ruan J. Structural preparation and biocompatibility evaluation of highly porous tantalum scaffolds. *Mater Lett*. 2013;100:152
- [11] Wauthle R, Stok JV, Yavari SA, Humbeeck JV, Kruth JP, Zadpoor AA, et al. Additively manufactured porous tantalum implants. *Acta Biomater*. 2015;14:217–25.
- [12] Kim Y, Kim E, Noh J, Lee S, Kwon Y, Oh IS. Fabrication and mechanical properties of powder metallurgy tantalum prepared by hot isostatic pressing. *IJRMHM*. 2015;48:211–16.
- [13] Papacci F, Rigante L, Fernandez E, Meglio M, Montano N. Anterior cervical discectomy and interbody fusion with porous tantalum implant: results in a series with long-term follow-up. *J Clin Neurosci*. 2016;33:159–62.
- [14] Kasliwal MK, Baskin DS, Traynelis VC. Failure of porous tantalum cervical interbody fusion devices: two-year results from a prospective, randomized, multicenter clinical study. *J Spinal Disord Tech*. 2013;26(5):239–45.
- [15] Mobb RJ, Phan K, Malham G, Seex K, Rao PJ. Lumbar interbody fusion: techniques, indications and comparison of interbody fusion options including PLIF, TLIF, MI-TLIF, OLIF/ATP, LLIF and ALIF. *J Spine Surg*. 2015;1(1):2–18.
- [16] Xu J, Xiao L, Zhang Y, Deng G, Liu G, Wu R, Shen H, Zhao X, Liu S, Cai Z. Ultra-high temperature oxidation resistance of a MoSi₂ composite coating with TaB₂ diffusion barrier on tantalum alloy. *Corros Sci*. 2023;224:111563.
- [17] Hao Y, Ye Z, Wang L, Ye M, Dong H, Du Y, Wang C. Dual-electrolyte fabrication of micro arc oxidation coatings on Ta–12W alloy with enhanced wear resistance. *Vacuum* 2023;211:111698.
- [18] Ma G, Zhao M, Xiang S, Zhu W, Wu G, Mao X. Effect of the severe plastic deformation on the corrosion resistance of a tantalum–tungsten alloy. *Materials*. 2022;15:7806.
- [19] Browning PN, Alagic S, Carroll B, Kulkarni A, Matson L, Singh J. Room and ultrahigh mechanical properties of field assisted tantalum alloys. *Mater Sci Eng A*. 2017;680:41–51.
- [20] Ma G, Wei Z, Wu G, Mao Z. *Mater Sci Eng A*. 2023;880:145312.
- [21] Wang L, Hu X, Ma X, Ma Z, Zhang Y, Lu Y, et al. *Colloids Surf B: Biointerfaces*. 2016;148:440–52.
- [22] Aguilar C, Martin FS, Martinez C, Camara B, Claverias F, Undabarrena A, et al. Improving mechanical properties and antibacterial response of α/β ternary Ti-Ta foams for biomedical uses. *J Mater Res Technol*. 2023;24:8735–53.
- [23] Kuo TY, Chin WH, Chien CS, Hsieh YH. Biocompatibility and corrosion of microplasma-sprayed titanium and tantalum coatings versus titanium alloy. *Surf Coat Technol*. 2019;372:399–409.
- [24] Mareci D, Chelariu R, Dan I, Gordin DM, Gloriant T. Corrosion behaviour of β -Ti20Mo alloy in artificial saliva. *J Mater Sci Mater Med*. 2010;21:2907–13.
- [25] Sharma M, Kumar AVR, Singh N, Adya N, Saluja B. Electrochemical corrosion behavior of dental/implant alloys in artificial saliva. *J Mater Eng Perform*. 2008;17:695–701.
- [26] Ho WF, Wu SC, Lin CW, Hsu SKHC. Electrochemical behavior of Ti-20Cr-X alloys in artificial saliva containing fluoride. *J Appl Electrochem*. 2011;41:337–43.
- [27] Oshida Y, Sellers CB, Mirza K, Farzin-Nia F. Corrosion of dental metallic materials by dental treatment agents. *Mater Sci Eng C*. 2005;25:343–8.
- [28] Lin FH, Hsu YS, Lin SH, Sun JS. The effect of Ca/P concentration and temperature of simulated body fluid on the growth of hydroxyapatite coating on alkali-treated 316L stainless steel. *Biomaterials*. 2002;23:4029–38.
- [29] Gurappa I. Characterization of different materials for corrosion resistance under simulated body fluid conditions. *Mater Charact*. 2002;49:73–9.
- [30] Okazaki Y, Gotoh E. Comparison of metal release from various metallic biomaterials in vitro. *Biomaterials*. 2005;26:11–21.

Received 2023-12-01

Accepted 2024-02-15